International Journal of Mechanical, Industrial and Aerospace Sciences
ISSN: 2517-9950
Vol:6, No:3, 2012

# Numerical Analysis of the Performance of the DU91-W2-250 Airfoil for Straight-Bladed Vertical-Axis Wind Turbine Application

M. Raciti Castelli, G. Grandi and E. Benini

***Abstract*—**This paper presents a numerical analysis of the performance of a three-bladed Darrieus vertical-axis wind turbine based on the DU91-W2-250 airfoil. A complete campaign of 2-D simulations, performed for several values of tip speed ratio and based on RANS unsteady calculations, has been performed to obtain the rotor torque and power curves. Rotor performances have been compared with the results of a previous work based on the use of the NACA 0021 airfoil. Both the power coefficient and the torque coefficient have been determined as a function of the tip speed ratio. The flow field around rotor blades has also been analyzed. As a final result, the performance of the DU airfoil based rotor appears to be lower than the one based on the NACA 0021 blade section. This behavior could be due to the higher stall characteristics of the NACA profile, being the separation zone at the trailing edge more extended for the DU airfoil.

***Keywords*—**CFD, vertical axis wind turbine, DU91-W2-250, NACA 0021

## I. Introduction and Background

THE need of renewable energy sources, which characterized the last decades, has became relevant thanks to the strong will of the European countries to cut carbon emissions by 20% and generate 34% of the total electricity consumption from renewables by 2020, with wind energy accounting for 14% [1]. In this scenario, the development of wind turbine technologies has allowed wind energy to perform a relevant step forward and the local production of clean electric power inside the built environment, such as industrial and residential areas, has led to a renewed interest in vertical axis wind turbines (VAWTs) for small-scale power generation [2] [3]. The main advantage of this particular rotor architecture consists in its omni-directionality: in fact, a VAWT can operate using wind coming from any direction, without requiring to be pointed; moreover, the maintenance of this type of wind generators appears to be less expansive with respect to classical architectures, due to the possibility of collapsing the turbine mast [4].

Marco Raciti Castelli is a Research Associate at the Department of Industrial Engineering of the University of Padua, Via Venezia 1, 35131 Padova, Italy (e-mail: marco.raciticastelli@unipd.it).

Giada Grandi is a M.Sc. student in Aerospace Engineering at the University of Padua, Via Venezia 1, 35131 Padova, Italy.

Ernesto Benini is an Associate Professor at the Department of Industrial Engineering of the University of Padua, Via Venezia 1, 35131 Padova, Italy (e-mail: ernesto.benini@unipd.it).

The DU91-W2-250 airfoil belongs to a class of wind turbine dedicated airfoils, developed by Delft University of Technology and is typically employed for horizontal axis wind turbine applications [5] [6] [7]. In the present work, the DU91-W2-250 airfoil has been applied to a three-bladed Darrieus vertical-axis rotor.

Several authors focused their works on the aerodynamics of VAWTs: in fact, some of the most complex phenomena in the field of Computational Fluid Dynamics (CFD) are associated with the simulation of the flow past rotating blades; besides, the aerodynamics of the Darrieus turbine is deeply influenced by the phenomenon of dynamic stall [8].

Ferreira et al. [9] focused on the numerical simulation of a single-bladed VAWT through the comparison with experimental measurements and PIV data, demonstrating that *DES* model is able to provide a good representation of the development of dynamic stall. Also Wang and Tao [10] performed a two-dimensional numerical investigation of the phenomenon of deep dynamic stall for a low Reynolds number flow over a NACA0012, comparing the *k-ω SST* model with low Reynolds number correction and the $v^2$-*f* model, finding that RANS approach is good for fast design or research of low Reynolds number airfoils, thanks to its capability of capturing a significant part of the flow dynamics.

Kumar et al. [11] proposed a low Reynolds number VAWT design and optimization procedure based on both CFD and BE-M calculations.

Raciti Castelli et al. [12] [13] presented a model for the evaluation of energy performance and aerodynamic forces on a single-bladed helical VAWT and also performed a validation campaign of a CFD code for a Darrieus micro-VAWT through a comparison with wind tunnel experimental data.

Again, Raciti Castelli and Benini [14] presented a two-dimensional CFD analysis of the influence of airfoil thickness on a straight-bladed Darrieus-type VAWT, performing a complete campaign of simulations based on full RANS unsteady calculations on a three-bladed rotor for two different blade profiles: NACA 0012 and NACA 0021. For each blade configuration, flow field characteristics were investigated and finally the rotor torque and power curves were compared for the two architectures, achieving a quantification of the effect of the blade thickness on overall rotor performance.

This paper focuses on a two-dimensional CFD analysis of a three-bladed Darrieus rotor, using the DU91-W2-250 airfoil. Numerical analysis have been performed through a full

campaign of simulations based on RANS unsteady calculations for eight different values of rotor tip speed ratio, defined as:

$$\lambda = \omega \cdot R_{rotor}/V_{\infty} \quad (1)$$

The purpose of the present work is to obtain rotor torque and power curves for the proposed blade section and also to compare the overall rotor efficiency with the classical NACA 0021 airfoil-based architecture investigated by Raciti Castelli et al. [15].

## II. Model Geometry

The main objective of this work is the numerical simulation of the aerodynamic behavior of a three-bladed Darreius vertical axis wind turbine characterized by the use of the DU91-W2-250 airfoil. Eight different angular velocities have been analyzed, while the unperturbed wind speed at computational domain entrance has been kept constantly equal to 9 m/s. Table I displays the geometrical and kinematic features of the tested rotor, while in Table II the main flow field characteristics are illustrated.

TABLE I
Main Geometrical Features of the Analyzed Rotor

| Denomination | Value |
|---|---|
| $D_{rotor}$ [mm] | 1030 |
| $H_{rotor}$ [mm] | 1 (2D simulation) |
| ω [rad/s] | 25.1÷57.6 |
| Blade section | DU91-W2-250 |
| c [mm] | 85.8 |
| N [-] | 3 |
| σ [-] | 0.5 |

TABLE II
Main Characteristics of the Simulated Flow Field

| Denomination | Value |
|---|---|
| p [Pa] | 101325 |
| ρ [kg/m3] | 1.225 |
| $V_{\infty}$ [m/s] | 9 |

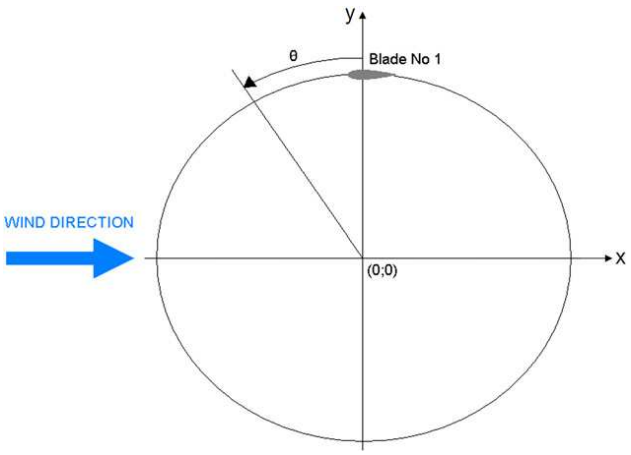


Fig. 1 Azimuthal coordinate of blade No. 1 centre of pressure

The solidity parameter was defined as:

$$\sigma = N \cdot c/R_{rotor} \quad (2)$$

where $R_{rotor}$ is rotor radius, as suggested by Strickland [16].

Rotor azimuthal position was identified by the angular coordinate of the pressure center of blade No.1 midsection (usually at 25% of the chord length), starting between the 2nd and 3rd Cartesian plane octants, as can be seen from Fig.1.

## III. Description of the Numerical Flow Field

The proposed numerical simulations aim to represent a turbine operating in open field conditions, hence it is necessary to consider a huge domain, essential to avoid solid blockage. The imposed conditions on the computational domain are the same which characterized all the previous works performed on similar rotor architectures [14] [15]. Fig. 2 displays the main geometrical features and dimensions of the computational domain, defined as *Wind Tunnel sub-grid*.

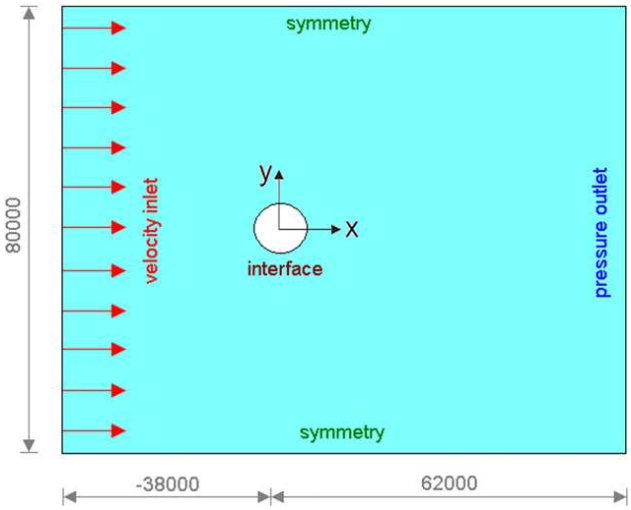


Fig. 2 Geometrical features and main dimensions [mm] of the computational domain

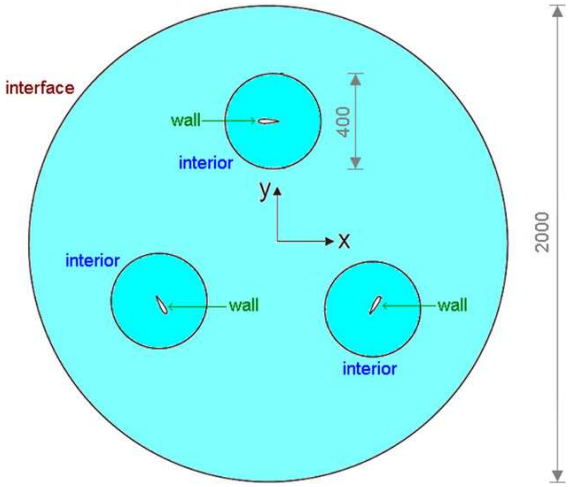


Fig. 3 Scheme of rotor sub-grid area [mm]

Inlet and outlet boundary conditions have respectively been placed 37 rotor diameters upwind and 60 rotor diameters downwind with respect to the rotor test section. Inlet has been set as a *velocity inlet*, with a constant wind velocity profile of 9 m/s, while outlet has been set as a *pressure outlet*. Two *symmetry* boundary conditions have been used for the two side walls. To ensure the continuity of the flow field, the circumference around the circular opening, centered on the turbine rotational axis, was set as an *interfac*e.

The inner zone of the flow field, named *Rotor sub-grid*, is exactly the area corresponding to the circular opening inside the *Wind Tunnel sub-grid*. This is the fluid area simulating the revolution of the wind turbine and is therefore characterized by a moving mesh, revolving at the same angular velocity of the rotor. Fig. 3 shows the main dimensions and the boundary conditions of the *Rotor sub-grid* area.

All the blade profiles inside the *Rotor sub-grid* area have been enclosed in a control circle of 400 mm diameter. This control area has no physical significance, being its purpose just to allow a precise dimensional control of the grid elements in the zone close to rotor blades. The mesh has been built by adopting a first size function operating from the blade profile to the control circle, and a second size function operating from the control circle to the whole *Rotor sub-grid* area, ending with grid elements of the same size of the corresponding *Wind Tunnel sub-grid* cells. An *interior* boundary condition was used for control circle borders, thus ensuring the continuity of the flow field on both sides of the grid.

## IV. Spatial Domain Discretization

An unstructured grid has been chosen for the whole computational domain, in order to reduce the engineering time to prepare the CFD simulations. The mesh on both sides of the *interface* (*Rotor sub-grid* and *Wind Tunnel sub-grid* areas) has approximately the same characteristic cell size, so as to obtain faster convergence.

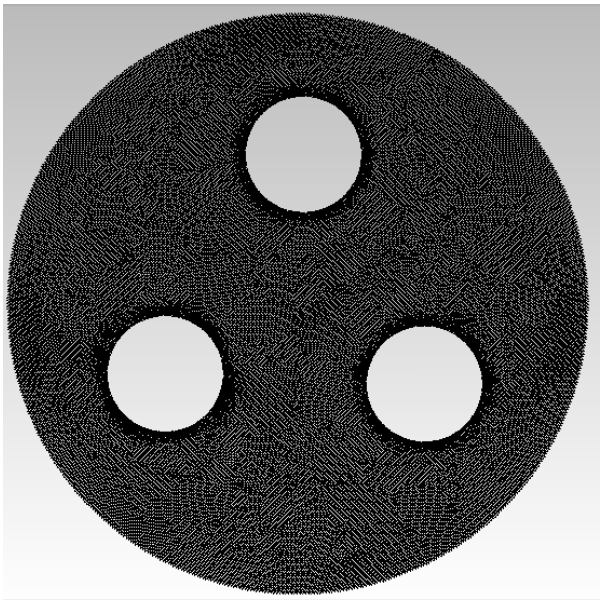

Fig. 4 Rotor sub-grid mesh for a three-bladed VAWT

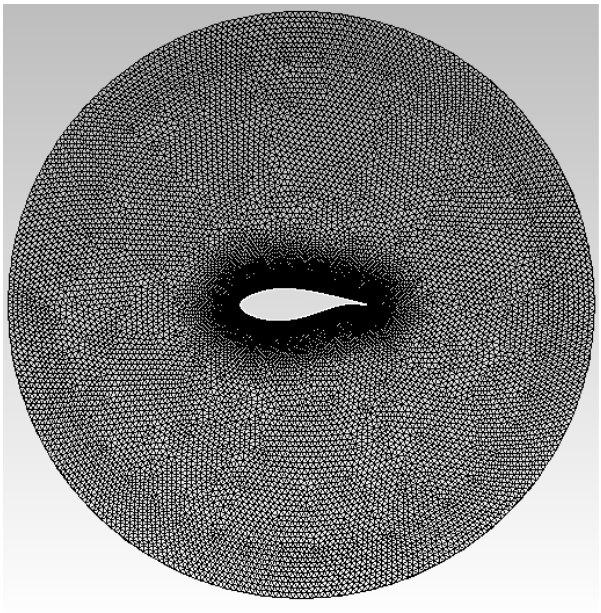

Fig. 5 Control circle grid for DU91-W2-250 blade section

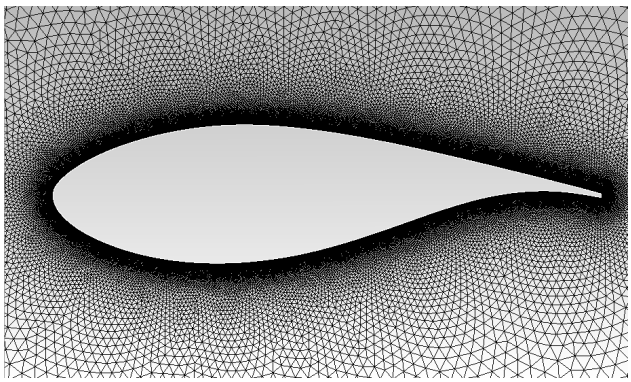

Fig. 6 Close up of the grid around the DU91-W2-250 airfoil

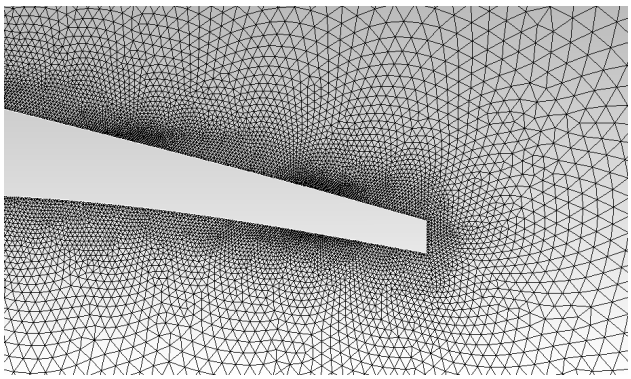

Fig. 7 Detail of the grid at the trailing edge of the DU91-W2-250 airfoil

An isotropic unstructured mesh has been chosen also for the *Rotor sub-grid*, in order to guarantee the same accuracy in the prediction of rotor performance during the revolution [17], and also in order to test the prediction capability of a very simple grid. Considering their features of flexibility and adaption

capability, unstructured meshes are in fact very easy to obtain, for complex geometries too, and often represent the "first attempt" in order to get a quick response from the CFD in engineering work. The *Rotor sub-grid* mesh is reproduced in Fig. 4.

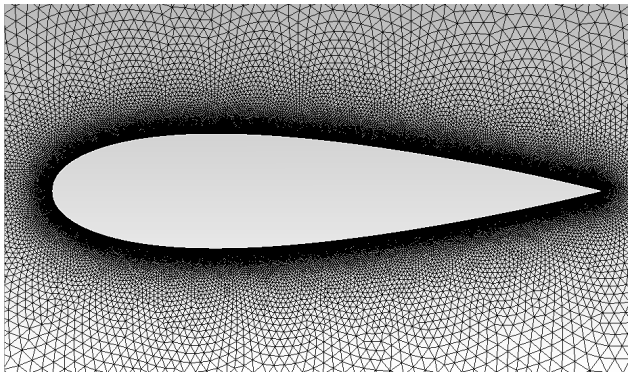

Fig. 8 Close up of the grid around the NACA 0021 airfoil

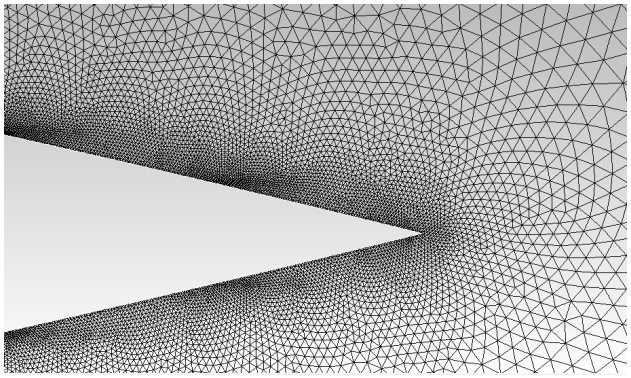

Fig. 9 Grid spacing at the trailing edge of the NACA 0021 airfoil

Being the area close to the blade profiles, great attention has been placed in the control circle. The computational grids have been constructed from lower topologies to higher ones, adopting appropriate size functions, in order to cluster grid points near the leading edge and the trailing edge of the blade profile, so as to improve the CFD code capability of determining lift, drag and the separation of the flow from the blade itself. Table III summarizes the main features of the mesh close to rotor blade. Fig. 5 represents the spatial grid distribution inside the control circle.

TABLE III
MAIN FEATURES OF THE MESH CLOSE TO ROTOR BLADE

| Denomination | Value |
|---|---|
| Number of grid points on airfoil upper/lower surface [-] | 3600 |
| Minimum grid spacing on airfoil leading edge [mm] | 0.015 |
| Minimum grid spacing on airfoil trailing edge [mm] | 0.025 |
| Growth factor from leading edge to airfoil trailing edge | 1.005 |
| Growth factor from airfoil surface to Rotor sub-grid area [-] | 1.1 |

In order to allow a comparison between the tested blade geometry and the reference NACA 0021 airfoil, Figs. from 6 to 9 show some features of the grids close to the two profiles, evidencing also some features of the spatial domain discretization close to the trailing edge.

## V. Characteristics of the Numerical Simulations

The tip speed ratio has been varied from a value of $\lambda$=1.44, (which corresponds to an angular velocity of $\omega$=25.1 rad/s) to $\lambda$=3.3 (corresponding to an angular velocity of $\omega$=57.6 rad/s). These conditions determine a range of Reynolds numbers from $3.2 \cdot 10^4$ to $7.4 \cdot 10^4$. As can be clearly seen, all of the presented computations concern low Reynolds number regimes.

## VI. Numerical Solution

The adopted commercial CFD solver is ANSYS FLUENT®, that implements 2-D Reynolds-averaged Navier-Stokes equations using a finite volume based solver. The fluid has been assumed to be incompressible, being the resultant maximum velocity in the order of 60 m/s. The temporal discretization has been achieved by imposing a physical time step equal to the lapse of time the rotor takes to make a 1 deg rotation. An improved temporal-discretization simulation did not show any significant variation [13]. As a global convergence criterion, each simulation has been run until instantaneous torque coefficient values have showed a deviation of less than 1% compared with the relative values of the previous period, corresponding to a rotation of 120°, due to rotor three-bladed geometry.

Residuals convergence criterion for each physical time step has been set to $10^{-5}$. The selected solver is a 2D pressure based, well suited to compute an incompressible flow field.

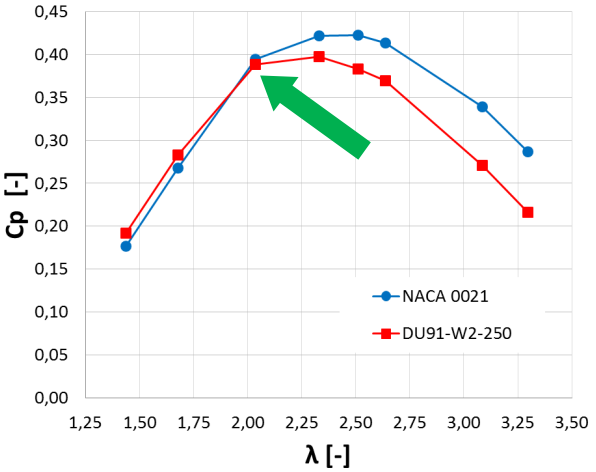


Fig. 10 Power coefficient as a function of tip speed ratio for the two considered blade sections

The *Realizable k-ε* model has been adopted for viscous computations. This model differs from the *Standard k-ε* in two points: it contains a new formulation for the turbulent viscosity and a new transport equation for the dissipation rate ε has been derived from an exact equation for the transport of the mean-

square vorticity fluctuations. One of the benefits of the *Realizable k-ε* model is that it provides superior performances for flows involving rotation, boundary layers under strong adverse pressure gradients, separation and recirculation.

## VII. Results and Discussion

Fig. 10 represents the evolution of the power coefficient $C_p$, defined as:

$$C_p = P / (½\cdot\rho\cdot A\cdot V_\infty^3) \quad (3)$$

as a function of the tip speed ratio for the two considered blade section architectures. It clearly appears how, for low values of the tip speed ratio, the DU91-W2-250 based rotor is able to perform slightly better than the NACA 0021 based one, while as λ approaches the value of 2 (emphasized by the green arrow), the DU-airfoil experiences a marked drop in performance. The percentage decrease of the peak power coefficient with respect to the reference NACA 0021 blade section is equal to 5.98%.

Fig. 11 represents the torque coefficient, defined as:

$$C_t = T/(½\cdot\rho\cdot A\cdot V_\infty^2 R) \quad (4)$$

as a function of the azimuthal coordinate θ.

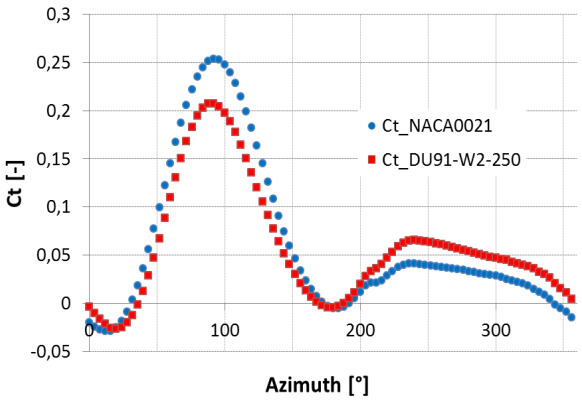


Fig. 11 Torque coefficient as a function of the azimuthal coordinate θ for the two considered blade sections

As can be clearly seen, the maximum values of the torque coefficient are registered for 92 deg angular coordinate, for both analized blade sections. It can also be noticed that the DU91-W2-250 airfoil presents lower performances during the upwind portion of blade revolution. On the contrary, it is able to surclass the NACA 0021 reference airfoil in the downwind positions. Nevertheless, the overall result is more favourable to the NACA airfoil (+5.98%).

Figs. 12 and 13 compare the contours of absolute velocity for the two considered rotor blade sections, for optimal tip speed ratio (λ = 2.33) and 92 deg azimuthal coordinate (peak of torque coefficient). A larger recirculation zone (evidenced by the red circle) is clearly visible at the trailing edge of the DU91-W2-250 airfoil, determining a descreased lift to trag ratio and a consequent loss of energy. Improved stall characteristics of the NACA 0021 with respect to the DU91-W2-250 airfoil appear to be the main responsible factors of the higher behavoir of the NACA-based blade architecture.

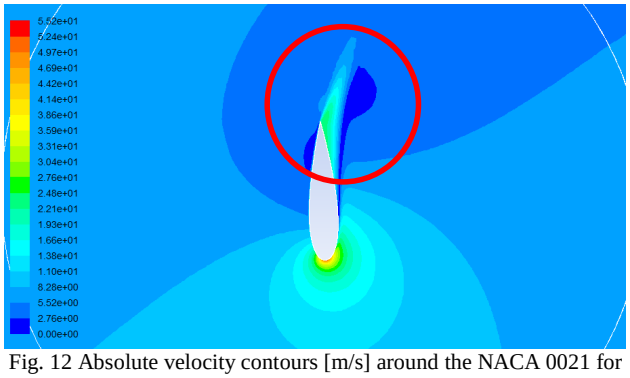

Fig. 12 Absolute velocity contours [m/s] around the NACA 0021 for 92 deg azimuthal position; λ = 2.33

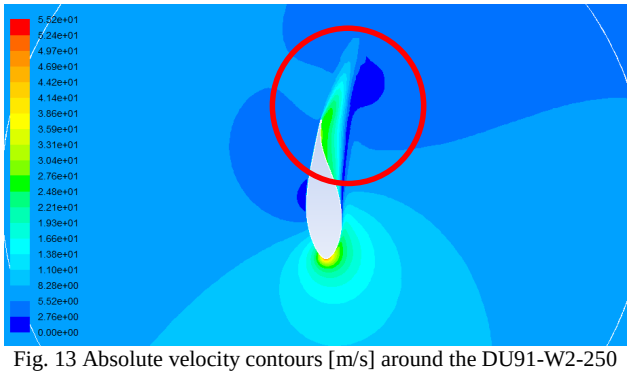

Fig. 13 Absolute velocity contours [m/s] around the DU91-W2-250 for 92 deg azimuthal position; λ = 2.33

## VIII. Conclusions and Future Works

The behavior of a DU91-W2-250 based Darrieus rotor has been investigated by means of a campaign of CFD simulations, performed for several values of tip speed ratio. Numerical predictions have been compared with previous results, obtained from a NACA 0021 based rotor. A significant decrease of the peak power coefficient has been registered: only for low values of the tip speed ratio, the DU91-W2-250 based rotor has proved able to perform slightly better than the NACA 0021 based one, while, for higher tip speed ratio values, the DU-airfoil has experienced a marked drop in performance. This phenomenon is probably to be connected with the lower stall characteristics of the DU91-W2-250 profile.

Further work should be done, in order to test the effect of blade curvature on the performance of a DU91-W2-250 based rotor.

## Nomenclature

| | |
|---|---|
| A [$m^2$] | rotor swept area |
| c [mm] | blade chord |
| $C_P$ [-] | wind turbine power coefficient |
| $C_t$ [-] | wind turbine torque coefficient |
| $D_{rotor}$ [mm] | rotor diameter |

| | |
|---|---|
| $H_{rotor}$ [mm] | rotor height |
| N [-] | rotor blade number |
| p [Pa] | air static pressure |
| P [W] | wind turbine power output |
| $R_{rotor}$ [mm] | rotor radius |
| T [Nm] | rotor torque |
| $V_\infty$ [m/s] | unperturbed wind velocity |
| θ [deg] | azimuthal coordinate |
| λ [-] | tip speed ratio |
| ρ [kg/m$^3$] | air density |
| σ [-] | rotor solidity |
| ω [rad/s] | rotor angular velocity |

## REFERENCES

[1] European Wind Energy Association, *EU energy policy after 2020*,www.ewea.org, 2011.

[2] A. S. Bahaj, L. Meyers and P. A. B. James, "Urban energy generation: Influence of micro-wind turbine output on electricity consumptions in buildings", *Energy and Buildings*, Vol. 39, Issue 2, February 2007, pp. 154-165.

[3] S. Mertens, *Wind Energy in the built environment*, Multiscience Publishing, 2006.

[4] W. Tong, W. Langreder, A. P. Schaffarczyk, S. G. Voutsinas, R. Z. Szasz, L. Fuchs, L. D. Willey, L. Staudt, P. Cooper, C. Lewis, T. Kanemoto, K. Kubo, D. Zheng, S. Bose, H. Matsumiya, B. F. Sorensen, J. W. Holmes, P. Brondsted, K. Branner, A. W. Hulskamp, H. E. N. Bersee, R. Hicks, B. Basu, J. van der Tempel, N. F. B. Diepeveen, D. J. Cerda Salzmann, W. E. de Vries, P. Milan, M. Wachter, S. Barth, J. Peinke, Y. Jiang, P. Pantazopoulou, M. Leahy, D. Connolly and N. Buckley, *Wind power generation and wind turbine design*, WIT Press, Southampton, UK, May 28, 2010.

[5] W. A. Timmer and R. P. J. O. M. van Rooij, "Summary of the delft university wind turbine dedicated airfoils", *AIAA-2003-0352*.

[6] W. A. Timmer and R. P. J. O. M. van Rooij, "Design of airfoils for wind turbine blades", *DUWIND, section Wind Energy, Faculty CiTG*, 3 May, 2004.

[7] M. Raciti Castelli, G. Grandi and E. Benini, "Numerical Analysis of Laminar to Turbulent Transition around DU91-W2-250 airfoil", submitted to *ICAFM 2012: International Conference on Advances in Fluid Mechanics*, Florence (Italy), February 28-29, 2012.

[8] I. Paraschivoiu, *Wind Turbine Design: With Emphasis on Darrieus Concept*, Polytechnic International Press, 2002.

[9] S. Ferreira, H. Bijl, G. van Bussel and G. van Kuik, "Simulating dynamic stall in a 2D VAWT: modeling strategy, verification and validation with particle image velocimetry data", *The Science of making torque from wind. Journal of Physics*: Conference Series 75, 2007.

[10] S. Wang, Z. Tao, L. Ma, D. Ingham and M. Pourkashanian, "Numerical investigations on dynamic stall associated with low Reynolds number flows over airfoils", *2nd International Conference on Computer Engineering and Technology (ICCET)*, Chengdu (China), 16-18 April, 2010.

[11] V. Kumar, M. Paraschivoiu and I. Paraschivoiu, "Low Reynolds number verical axis wind turbine for Mars", *Wind Engineering*, Vol. 34, No. 4, June 2010.

[12] M. Raciti Castelli and E. Benini, "Effect of blade inclination angle on a Darrieus Wind Turbine", *Journal of turbomachinery*, October 2011, Vol 133.

[13] M. Raciti Castelli, G. Pavesi, E. Benini, L. Battisti and G. Ardizzon, "Modeling strategy and numerical validation for a Darrieus vertical axis micro-wind turbine", *Proceedings of the ASME 2010 International Mechanical Engineering Congress & Exposition*, November 12-18 2010, Vancouver, British Columbia, IMECE2010-39548.

[14] M. Raciti Castelli and E. Benini, "Effect of blade thickness on Darrieus Vertical-Axis Wind turbine performance", *CSSim 2011, 2nd International Conference on Computer Modelling and Simulation*, 5-7 September 2011, Brno (Czech Republic).

[15] M. Raciti Castelli, A. Englaro and E. Benini, "The Darrieus wind turbine: Proposal for a new performance prediction model based on CFD", *Energy* 36 (2011), pp. 4919-4934.

[16] J. H. Strickland, "The Darrieus turbine: a performance prediction model using multiple streamtube", *SAND75*, 2007.

[17] R. M. Cumming, J. R. Forsythe, S. A. Morton and K. D. Squires, "Computational challenges in high angle of attack flow prediction", *Progr Aerosp Sci* 2003; 39(5):369-84.